Three-dimensional vesicles under shear flow: Numerical study of dynamics and phase diagram

Thierry Biben,[1] Alexander Farutin,[2] and Chaouqi Misbah[2]

[1]*Université de Lyon, F-69000, France; Université Lyon 1, Laboratoire PMCN, CNRS UMR 5586, F-69622 Villeurbanne Cedex, France*

[2]*Université de Grenoble and CNRS, Laboratoire Interdisciplinaire de Physique, UMR5588, 140 Avenue de la Physique, F-38402 Saint Martin d'Hères, France*

(Received 15 December 2009; revised manuscript received 12 November 2010; published 30 March 2011)

The study of vesicles under flow, a model system for red blood cells (RBCs), is an essential step in understanding various intricate dynamics exhibited by RBCs *in vivo* and *in vitro*. Quantitative three-dimensional analyses of vesicles under flow are presented. The regions of parameters to produce tumbling (TB), tank-treating, vacillating-breathing (VB), and even kayaking (or spinning) modes are determined. New qualitative features are found: (i) a significant widening of the VB mode region in parameter space upon increasing shear rate $\dot{\gamma}$ and (ii) a robustness of normalized period of TB and VB with $\dot{\gamma}$. Analytical support is also provided. We make a comparison with existing experimental results. In particular, we find that the phase diagram of the various dynamics depends on three dimensionless control parameters, while a recent experimental work reported that only two are sufficient.

DOI: 10.1103/PhysRevE.83.031921 PACS number(s): 87.16.D−, 83.50.Ha, 83.80.Lz, 87.17.Jj

I. INTRODUCTION

Vesicles, which are made of a pure bilayer of phospholipids, are regarded as an elementary system for the understanding of individual red blood cells (RBCs) dynamics, a first step toward a bottom-up approach to blood flow and rheology. Apart from a dilute suspension where a rheological law can be extracted analytically [1], a complete understanding of blood flow should ultimately emerge from a numerical study.

Computational approaches are, however, challenging due to the free boundary character of the RBCs; the shape is not known *a priori* and is fixed via a subtle interplay between the local flow and the different internal modes of the RBCs (membrane bending, shear elasticity). To date, several numerical studies have been devoted to the study of vesicles, capsules, or RBCs [2–12].

Our goal in this paper is to present numerical simulation for a single three-dimensional vesicle under shear flow in the Stokes limit with an arbitrary viscosity contrast. We determine the range of parameters (control and material parameters) corresponding to different dynamics of vesicles. It will emerge that even for such an apparently simple situation the full phase diagram reveals several unexplored features.

RBCs, apart from having the same type of phospholipid membrane as vesicles, are endowed with a cytoskeleton (a cross-linked network of proteins lying underneath the RBC membrane). Nevertheless, their dynamics seem to share some common properties with vesicles. Under simple shear flow, RBCs [13] and vesicles [14–16] exhibit *tank-treading* (TT) and *tumbling* (TB); these two modes have been studied both theoretically and numerically [2,4,17,18]. More recently, a new type of motion called *vacillating-breathing* (VB) (a.k.a. swinging or trembling) has been both predicted [19–23] and observed experimentally [16,24]. In this mode the main axis of the vesicle oscillates about the flow direction, whereas its shape makes a breathing motion (see movies [25]). VB has also been observed for capsules, which are, like RBCs, endowed with membrane shear elasticity [11]. Another motion observed for vesicles, called spinning in Ref. [21], is also characterized here (see the movie for this type of motion [25]). This motion was described for rigid ellipsoids by Jeffery [26]; the main axis describes a cone about the perpendicular to the plane of the shear flow (see movies [25]). Unlike rigid particles where the cone angle is fixed by initial conditions (due to the reversibility of the Stokes equations), the cone angle for vesicles is an intrinsic property. This kind of motion is rather known under the name kayaking (K) in other fields (e.g., rigid particles, polymers, liquid crystals); we thus adopt the term kayaking to comply with the common usage [27]. A systematic analysis of these four motions (TT, TB, VB, K) is explored in this paper.

Previous analytical and numerical studies have reported on the phase diagram of the various motions. The first important result to be reported here is that even for a quasispherical shape, the location of the transition boundary between TT and TB is significantly overestimated by previous analytical results. We explain briefly here the main reason. The second important result is that the band of the phase diagram where the VB mode takes place (in parameter space) widens upon increasing the shear rate. It seems that this widening was not reported previously, neither analytically nor numerically and experimentally. We shall also show that K seems to occur even if the vesicle is initially forced to be in the shear plane. In other words, TB vesicles undergo a transverse instability. A final result is that we find that the period of oscillation (defined as the time needed for the major axis to make a full rotation) in the TB regime (rescaled by the shear rate) is quite insensitive to the shear rate, in good agreement with the Keller-Skalak (KS) theory [17].

This paper is organized as follows. In Sec. II we present the model equation for vesicles in the Stokes limit. In Sec. III we provide the basic ingredients of the numerical method together with some typical results related to convergence and precision. In Sec. IV we present the major results of the present study. Sections V and VI are devoted to comparison with experimental results. Section VII contains a conclusion and some general remarks.

II. THE MODEL

We consider a model system, which is a phospholipid vesicle (Fig. 1). The Stokes equations (experiments have so

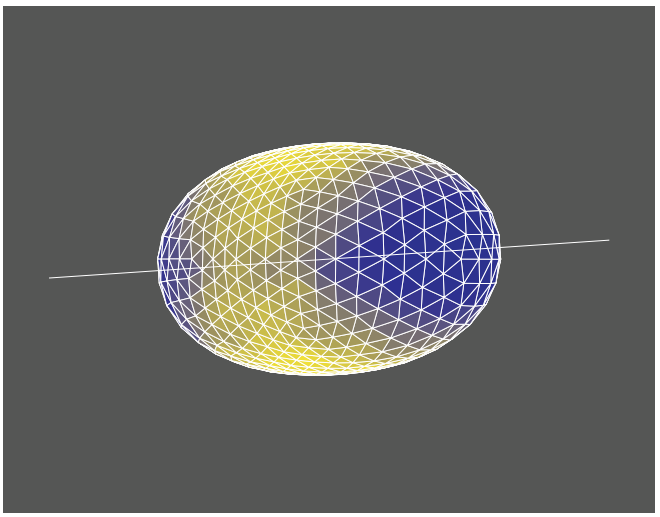

FIG. 1. (Color online) A typical vesicle obtained by simulations. The white line indicates the main axis direction. The color code on the vesicle corresponds to the value of the local curvature, which is large at the tips and low in the central region.

far explored the limit of small Reynolds numbers) can be formally solved using the boundary integral (BI) formalism (see, for example, [28]) which yields

$$\eta_m \mathbf{v}_{\rm mem}(\mathbf{r}) = \eta_{\rm out}\mathbf{v}_{\rm shear}(\mathbf{r}) + \int_{\rm mem} \overline{G}(\mathbf{r}-\mathbf{r}')\mathbf{f}_{\rm mem}(\mathbf{r}')\,d\mathbf{r}' + (\eta_{\rm out}-\eta_{\rm in})\int_{\rm mem} \mathbf{v}_{\rm mem}(\mathbf{r}')\cdot\overline{K}(\mathbf{r}-\mathbf{r}')\cdot\hat{\mathbf{n}}(\mathbf{r}')\,d\mathbf{r}', \quad (1)$$

where $\mathbf{v}_{\rm mem}(\mathbf{r})$ is the local velocity field at the membrane, $\mathbf{v}_{\rm shear} = \dot{\gamma}\, y\hat{\mathbf{x}}$ is the externally applied Couette flow (with $\dot{\gamma}$ the shear rate), $\eta_m \equiv (\eta_{\rm in}+\eta_{\rm out})/2$ ($\eta_{\rm in}$ and $\eta_{\rm out}$ stand for viscosities of the internal and external fluid, respectively), $\int_{\rm mem}$ is an integration over the membrane, $\hat{\mathbf{n}}$ is the outward unit normal vector, and $\overline{G}(\mathbf{r}-\mathbf{r}')$ and $\overline{K}(\mathbf{r}-\mathbf{r}')$ are the Green's tensors defined as

$$\overline{G}(\mathbf{x})_{ij} = \frac{1}{8\pi}\left(\frac{\delta_{ij}}{x} + \frac{x_i x_j}{x^3}\right); \quad \overline{K}(\mathbf{x})_{ijk} = \frac{3}{4\pi}\frac{x_i x_j x_k}{x^5}. \quad (2)$$

A vesicle that is subjected to a flow undergoes a shape transformation that is limited by bending modes. The reaction bending force of a vesicle on the fluid is given by the Helfrich force [29]

$$\mathbf{f}_{\rm curv}(\mathbf{r}) = -\kappa\left[\tfrac{1}{2}c(\mathbf{r})\{c(\mathbf{r})^2 - 4g(\mathbf{r})\} + \Delta_{2D}c(\mathbf{r})\right]\hat{\mathbf{n}}(\mathbf{r}), \quad (3)$$

where κ is the bending modulus, $c(\mathbf{r})$ is the local mean curvature [$c(\mathbf{r}) = c_1(\mathbf{r}) + c_2(\mathbf{r})$, where c_1 and c_2 are the two principal curvatures at point $\mathbf{r}$ of the membrane], $g(\mathbf{r})$ is the Gaussian curvature ($g = c_1c_2$), and Δ_{2D} is the (surface) Laplace-Beltrami operator on the membrane. The other contribution to the membrane force follows from local membrane incompressibility:

$$\mathbf{f}_{\rm tens}(\mathbf{r}) = \mathcal{T}[\zeta(\mathbf{r})c(\mathbf{r})\hat{\mathbf{n}}(\mathbf{r}) + \nabla_{2D}\zeta(\mathbf{r})], \quad (4)$$

where ∇_{2D} is the surface gradient operator and $\zeta(\mathbf{r})$ is a local dimensionless Lagrange multiplier that enforces membrane inextensibility (the constant $\mathcal{T}$ has a dimension of energy per unit surface). Local membrane inextensibility sets severe limitations on the numerics, on both the time step and the precision of the results, as discussed in the next section.

III. THE NUMERICAL METHOD

The numerical procedure is simple in its principle: From the shape of the vesicle we can compute the membrane force $\mathbf{f}_{\rm mem}$. The knowledge of $\mathbf{f}_{\rm mem}$ allows us to get the expression of the velocity field at the membrane interface thanks to the integral formulation (1) and thus to predict its motion. We refer to [28] for the general description of the BI method; however, specific schemes have been used to solve particular problems that we discuss now.

A. The mesh

The mesh is defined using an elementary icosahedron. This icosahedron is refined by dividing each of its triangular faces into four triangles (the new vertices corresponds to the middles of the edges). This refinement can be applied recursively until the expected degree of accuracy is reached (we do it three times so that we end with 642 vertices and 1280 triangles). The resulting mesh is projected on a unit sphere that can be stretched or flattened to obtain a prolate or oblate ellipsoid. Noise is added to the mesh to remove an eventual excess of symmetry at particular sites. Examples are provided in Fig. 2 where we show the mesh used for a spherical vesicle and the initial ellipsoidal configuration for a prolate vesicle.

B. Advection of the mesh

The basic advection scheme, using the velocity field to calculate the new position of the vertices, is not appropriate to the problem we consider here. Indeed, when the vesicle tanktreads, the differential motion between the points located in the equatorial region and the vertices located close to

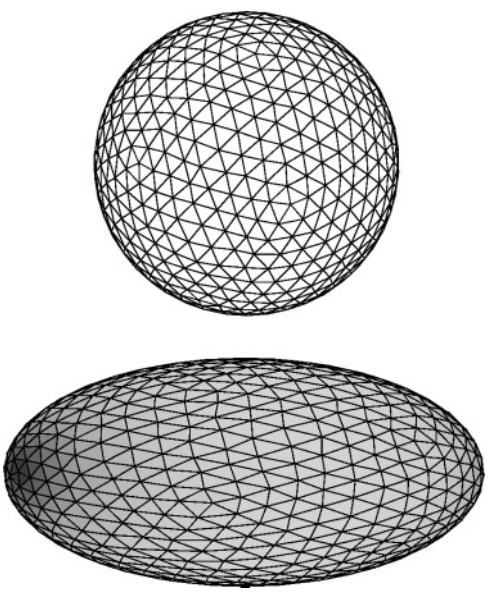

FIG. 2. Example of mesh used for a spherical and ellipsoidal initial configuration. For the ellipsoidal shape, the gray scale corresponds to the local curvature field.

the rotation pole results in an entanglement of the mesh after few rotations. These entanglements induce numerical instabilities and must be avoided. Several techniques can be used to prevent these instabilities, like regenerating the mesh from time to time. These regeneration steps are not innocuous: They introduce noise and discontinuities in the dynamics since the position of the new vertices is obtained by interpolation or extrapolation. Another solution is to replace the basic advection scheme with a more efficient one, keeping in mind that the mesh is essentially defined to trace the shape of the vesicle: The mesh points are not supposed to follow the actual dynamics of matter; they only need to follow it in the normal direction. More precisely, the knowledge of the normal velocity is sufficient to determine the new shape. We can thus remove the tangential component of the velocity at the surface of the vesicle in order to compute the dynamics of the vertices. Let us first define the velocity of a vertex in the frame of the center of mass of the vesicle as

$$\mathbf{u}(\mathbf{r}) = \mathbf{v}(\mathbf{r}) - \mathbf{v}_{\text{c.m.}}, \tag{5}$$

where $\mathbf{r}$ denotes the position of a vertex and $\mathbf{v}_{\text{c.m.}}$ is the velocity of the center of mass of the vesicle. In the center-of-mass frame, the advection velocity for a vertex is

$$\mathbf{u}_{\text{adv}}(\mathbf{r}) = \mathbf{u}(\mathbf{r}) \cdot \hat{\mathbf{n}}(\mathbf{r})\, \hat{\mathbf{n}}(\mathbf{r}), \tag{6}$$

and in the laboratory frame, it becomes

$$\mathbf{v}_{\text{adv}}(\mathbf{r}) = \mathbf{u}(\mathbf{r}) \cdot \hat{\mathbf{n}}(\mathbf{r})\, \hat{\mathbf{n}}(\mathbf{r}) + \mathbf{v}_{\text{c.m.}}. \tag{7}$$

The advection equation for a vertex $\mathbf{r}_i$ of the mesh is thus

$$\mathbf{r}_i(t + dt) = \mathbf{r}_i(t) + \mathbf{v}_{\text{adv}}(t)\, dt. \tag{8}$$

Using this prescription, it is possible to obtain a mesh that reaches a steady state while the vesicle is TT. In this case, entanglements are suppressed automatically. One can consider this scheme as a continuous regeneration of the mesh of the vesicle. Of course, while the mesh (which is a pure geometrical representation of the shape) does not follow the dynamics of matter in the tangential directions, physical fields transported at the surface of the vesicle by the velocity field have to be advected by the full velocity. As an example of a physical field, consider the case of the tension field $\zeta(\mathbf{r})$, we must use the convective derivative

$$\frac{D\zeta}{Dt} = \frac{\partial \zeta}{\partial t} + \mathbf{v}_{\text{t}}.\nabla_{2D}\zeta \tag{9}$$

to calculate the variation of ζ at a vertex of the mesh, where $\mathbf{v}_{\text{t}}(\mathbf{r}) = \mathbf{v}(\mathbf{r}) - \mathbf{v}_{\text{adv}}(\mathbf{r})$ is the tangential component of $\mathbf{u}(\mathbf{r})$, and ∇_{2D} is the gradient along the surface. We require local membrane incompressibility. If we view ζ as a tension force, a possible small (see below for the specification of the smallness) compression or dilation of the local area induces a tension that is (to leading order) proportional to the change of area. Since ζ is advected, we write the evolution equation for ζ as

$$\frac{\partial \zeta(\mathbf{r})}{\partial t} + \mathbf{v}_{\text{t}} \cdot \nabla_{2D}\zeta(\mathbf{r}) = \frac{1}{A(\mathbf{r})}\frac{dA(\mathbf{r})}{dt} \tag{10}$$

with this scheme. $A(\mathbf{r})$ is the area element attributed to site $\mathbf{r}$ (1/3 of the sum of the area of the triangles containing $\mathbf{r}$) and the temporal variation $\frac{dA(\mathbf{r})}{dt}$ is calculated using the *full* velocity field. The right-hand side of the equation is also equal to the surface divergence of the velocity field. Exact incompressibility would require a vanishing surface divergence. Equation (10) can be viewed as a penalization procedure (the full tension is $\mathcal{T}\zeta$, as is visible from the definition of the force, Eq. (4), with $\mathcal{T}$ a large parameter; see below), where the surface divergence scales as the tension divided by $\mathcal{T}$. This enforces a very small surface divergence. We show below (in the Sec. III D) how the local area is conserved in practice.

When the vesicle tumbles, this advection scheme in the normal direction reduces mesh entanglements, but does not entirely suppress them, so we have to regenerate the mesh from time to time in the same way we constructed the initial configuration: A spherical mesh centered on the vesicle is generated whose vertices are projected on the actual shape. The time t_{mesh} between two regenerations of the mesh is a control parameter; we use in practice $\gamma t_{\text{mesh}} = 1$, but we also tried different values as well as random regeneration times, with minor influence on the results if t_{mesh} remains smaller than the TB period. In this case, the discontinuities induced in the dynamics are barely measurable.

C. Curvature and differential operators

On a triangulated surface these operators can be estimated at each vertex as follows. The Laplace-Beltrami operator applied to a function $f_i \equiv f(\mathbf{r}_i)$ defined at any vertex $\mathbf{r}_i$ of the surface can be estimated as [30]

$$\Delta_{2D} f = \frac{1}{2A_i}\sum_{j\in n_i}(\cot\alpha_{ij} + \cot\beta_{ij})\,(f_j - f_i), \tag{11}$$

where i denotes the site where the Laplace-Beltrami operator is computed, n_i represents the set of neighboring sites [connected to site i by a link; see Fig. 3 (left)]. α_{ij} and β_{ij} are the two angles defined in Fig. 3 (left) and A_i is the area attributed to site i, that we can compute by summing over all the triangles containing the site i, a third of their area. The local curvature at site i can be derived from this expression by replacing the function $f(\mathbf{r}_i)$ by $-\mathbf{r}_i$. Let us define the curvature vector as

$$\mathbf{K} = \frac{1}{2A_i}\sum_{j\in n_i}(\cot\alpha_{ij} + \cot\beta_{ij})\,(\mathbf{r}_i - \mathbf{r}_j). \tag{12}$$

The local curvature at the surface of the vesicle is

$$\begin{aligned} c(\mathbf{r}_i) = c_1(\mathbf{r}_i) + c_2(\mathbf{r}_i) = -\|\mathbf{K}\| \quad &\text{if} \quad \mathbf{K}\cdot\hat{\mathbf{n}} > 0 \\ + \|\mathbf{K}\| \quad &\text{otherwise,} \end{aligned} \tag{13}$$

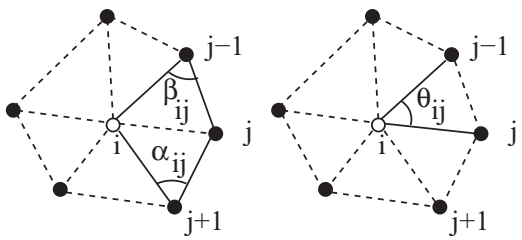

FIG. 3. Angle definitions for the Laplace-Beltrami operator computation (left) and Gaussian curvature (right).

where $\hat{\mathbf{n}}$ is the normal vector pointing toward the external medium. A sphere shall thus have a negative curvature with these conventions.

The computation of the Gaussian curvature is simpler, from its definition it can be estimated as

$$g(\mathbf{r}_i) = \frac{2\pi - \sum_{j\in n_i} \theta_{ij}}{A_i}, \tag{14}$$

where θ_{ij} is defined in Fig. 3 (right).

The surface gradient operator ∇_{2D} of a function at a vertex $\mathbf{r}_i$ can be estimated by averaging the gradient calculated on the neighboring triangles (the triangles containing i). The average is weighted by the area of the triangle, and the gradient is calculated in each triangle by assuming a linear form for the function inside the triangle.

D. Area conservation

Area conservation is an important constraint on the dynamics of vesicles as discussed by Helfrich in his seminal article [31]. Equation (10) is able to fix the area of the vesicle within a few percent in usual cases. This accuracy is unfortunately not sufficient to obtain reliable results in general, especially when the vesicle tumbles and is subjected to a cyclic stress. In such a case the area of the membrane oscillates around an average value and these oscillations can modify the dynamics. This problem is particularly important for quasispherical vesicles, the case usually considered in analytical works. Indeed, the limit of a spherical shape presents a peculiarity: There is no distinction between TT and TB. As a consequence, the TB regime disappears abruptly in this limit. The dynamics of a vesicle is thus very sensitive to the value of the reduced volume,

$$\tau = 6\sqrt{\pi}V/S^{3/2}, \tag{15}$$

that controls its shape (V is the volume of the vesicle and S its area). The maximum value $\tau = 1$ corresponds to a sphere, while $\tau = 0.95$ is still small for most analytical approaches. Fixing τ with an accuracy better than 1% is thus a key point in this study. Fortunately, a quasiperfect adjustment can be obtained with the help of a very simple feedback on the tension field ζ,

$$\left.\frac{\partial \zeta(\mathbf{r})}{\partial t}\right|_{\text{feedback}} = \alpha(\tau - \tau_{\text{sim}}) - \xi\frac{\partial \tau_{\text{sim}}}{\partial t}, \tag{16}$$

that we can add to the right-hand side of (10). Here τ_{sim} is the instantaneous reduced volume of the vesicle and τ is the requested value. α and ξ are two positive constants that fix the relaxation time of τ_{sim} to its expected value τ. The last term $d\tau_{\text{sim}}/dt$ is a damping term that prevents the scheme from spurious oscillations. The scheme used in this study ensures a variation of τ (and thus S) lower than 6×10^{-6} for any of the results presented in this article. We show in Fig. 4 the variation of τ in the TB regime for the most difficult case we considered (due to the proximity of a transition line). We can clearly see the efficiency of the scheme and the stability of the overall method, which makes it possible to follow the vesicle during several hundred TB periods.

The numerical control parameters are chosen as follows. α is a frequency and ξ is dimensionless. We used $t_{\text{curv}} = \eta_{\text{out}}R^3/\kappa$ as the time unit in our simulation; this is the characteristic relaxation time of a vesicle in a quiescent fluid. If R is the typical radius of the vesicle, defined as $R \equiv (3V/4\pi)^{1/3}$, then we choose the parameter values according to the following relations:

$$\alpha = 10^5/t_{\text{curv}}, \quad \xi = 10^3, \quad \mathcal{T} = 5000\kappa/R^2. \tag{17}$$

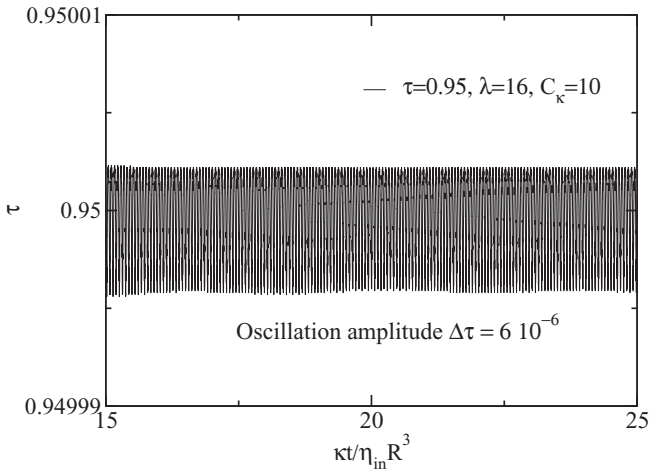

FIG. 4. Oscillations of the reduced volume in the TB regime. The variations of τ remain very weak thanks to the feedback added to the tension field ζ.

IV. RESULTS

The phase diagram of various dynamics (TT, TB, and VB) of a vesicle and RBC in a Couette flow recently motivated a large number of theoretical and experimental studies [1,21,22,32–34]. This is the first focus of our study. Let us introduce appropriate dimensionless numbers. Shape deformability can be measured by the dimensionless number

$$C_\kappa = \frac{\eta_{\text{out}}\dot{\gamma}R^3}{\kappa} \equiv \dot{\gamma}t_{\text{curv}}. \tag{18}$$

Vesicles exhibit various equilibrium shapes (i.e., in the absence of flow) [35], depending on their reduced volume τ. τ is the second dimensionless parameter. For $\tau > 0.652$, the shape is prolate (one long revolution axis) [35]. In the range $0.591 < \tau < 0.652$, the shape is oblate (one small revolution axis; the shape is biconcave, known also for RBCs). We found that, for $C_\kappa \geqslant 1$ (which is quite easily reachable experimentally), the oblate branch is suppressed in a Couette flow so that only prolate shapes prevail (see Fig. 1). This result agrees with that of Noguchi and Gompper [36]. The last dimensionless parameter is the ratio of the internal fluid viscosity over that of the external one:

$$\lambda = \eta_{\text{in}}/\eta_{\text{out}}. \tag{19}$$

We first focus on a reduced volume close enough to unity. This will allow us to compare our results to the theoretical ones considering the quasispherical limit [19–23]. We have chosen the value $\tau = 0.95$ and have explored the effects of the two other parameters C_κ and λ. The resulting phase diagram is represented in Fig. 5.

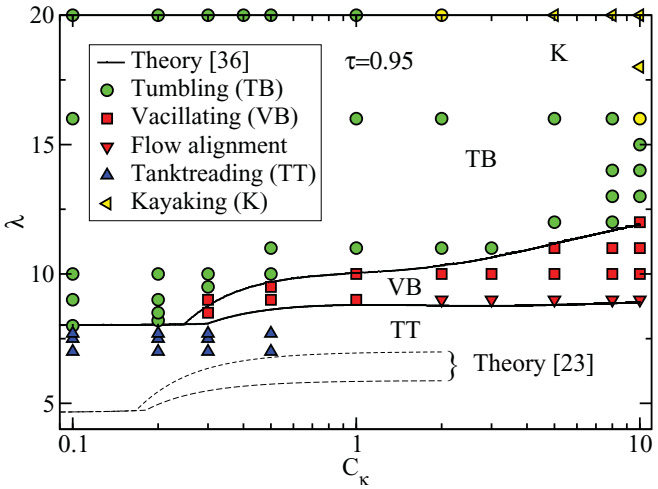

FIG. 5. (Color online) Phase diagram for $\tau = 0.95$ (corresponding to an excess area $\Delta = S/R^2 - 4\pi = 0.43$, where S is the area of the vesicle, and the radius R is defined from the volume V as $3\pi R^3/4 = V$). The symbols correspond to numerical results, the solid line to the analytical ones of Farutin *et al.* [37], and the dashed lines to the theory of Danker *et al.* [23]. The flow alignment states correspond to a VB mode with a very small amplitude (see Fig. 13). These states are thus intermediate between VB and TT. The K phase is visible at the upper right corner of the diagram.

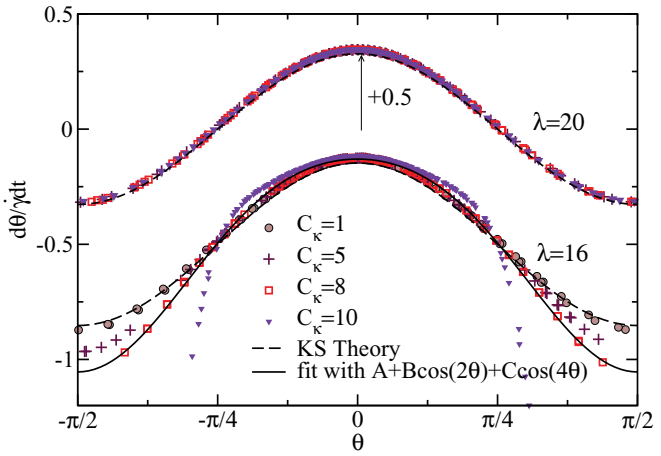

FIG. 6. (Color online) $\dot{\theta}$ as a function of θ for $\lambda = 16$, $\lambda = 20$ (shifted upward by $+0.5$), for various C_κ. The dashed line corresponds to the KS theory. The solid black line is a fit of the data points for $\lambda = 16$ and $C_\kappa = 8$ with the function $A + B\cos(2\theta) + C\cos(4\theta)$ ($A = 0.543$, $B = 0.462$, and $C = 0.049$), showing that higher harmonics play an important role.

A first important feature found here is that the boundaries of the phase diagram are strongly underestimated in previous analytical theories [21,23]. For example, for $C_\kappa \simeq 0.1$, the bifurcation from TT to TB occurs here for $\lambda \simeq 8$, while analytical theories predicted $\lambda \simeq 4$ (Fig. 5). This is unexpected because deviation from a sphere is only about 5% and a perturbative scheme is expected to make sense. Thus, we have attempted to understand this behavior by revising previous analytical theories. The key ingredient is that the next order terms in an expansion in powers of excess area (relative to a sphere) are decisive, however small the deviation from a sphere is. We have identified the fact that this is the result of a singular behavior of the expansion scheme. Details of the analytical theory are given elsewhere [37]. The outcome of this analytical theory is presented in Fig. 5, revealing excellent agreement with the full numerical simulation.

Previous analytical [21,23] as well as numerical calculations [22] (based on hybrid simulations of a dynamically triangulated membrane model and a particle-based mesoscale solvent, multiparticle collision dynamics) and experiments [32] reported that the band of existence of the VB mode saturates with C_κ above a value of the order of $C_\kappa \sim 0.5$. This is in good agreement with the present numerical study as long as $0.5 < C_\kappa < 2$. Beyond a value of the order of $C_\kappa = 2$, the VB band exhibits a sudden ample widening, as shown in Fig. 5. This effect highlights the nontrivial character of dynamics due to shape deformation. A careful theoretical analysis of this phenomenon has led us to the discovery that not only is the fourth-order harmonic strongly coupled to the second one, but it also acquires strong activity on increasing C_κ. This mode, which is damped at low deformability, becomes active (i.e., it is excited) at larger deformability (larger C_κ). As a consequence, the VB regime is promoted, leading to the VB band widening. We have found that this behavior is captured by the new theory that implements fourth-order harmonics [37].

Let us now analyze the behavior of the TB angle $\theta(t)$. It is convenient to represent a phase portrait in the plane $(\dot{\theta},\theta)$. This will also allow us to shed light on the limit of applicability of the KS theory, which is often used as a basis in experiments [15,16] and in numerical simulations [22]. We find that, for $C_\kappa \to 0$ (we choose $C_\kappa = 0.1$ as an example), the simple relation $\dot{\theta}/\dot{\gamma} = A + B\cos(2\theta)$ (where A and B depend on the geometrical properties of the ellipsoid and on the viscosity ratio λ, as described in Ref. [17]) predicted by the KS theory is in excellent agreement with the BI simulations.

At larger deformabilities, the situation is more complex and requires a careful analysis. We first focus on the value $\lambda = 20$. The result is reported in Fig. 6 (shifted by $+0.5$ upward for clarity). All data for $1 < C_\kappa < 10$ are nearly superimposed, reflecting a good agreement with the KS theory even though, for $C_\kappa \geqslant 5$, the vesicle is actually K (Figs. 7 and 8). $\theta(t)$ represents the TB of the projection of the main axis in the shear plane. In contrast, at smaller values of λ ($\lambda = 16$ in Fig. 6), significant deviations from the KS theory are manifested. In particular, we observe the excitation of the fourth-order harmonic, represented by $\cos(4\theta)$ in the figure when C_k is increased up to 8. Note that, for $C_\kappa = 10$, other higher-order harmonics are excited as well, which is a precursor to the TB-VB or the TB-K bifurcation.

We find that K takes place at much larger values of λ than reported in [21], and we did not see evidence for coexistence with TB. Figure 8 shows a typical behavior of the two K angles. Note, finally, that all spherical harmonics of odd and even orders are free to develop in the numerical scheme. We have checked that odd harmonics (such as third-order harmonics) are absent from dynamics. If noise were present, it may induce odd harmonics (like third harmonic observed in experiments [32]), but the effect of noise is beyond the present study.

Another fact is the quasirobust character of the rescaled period (Fig. 9) as a function of the deformation regardless of the

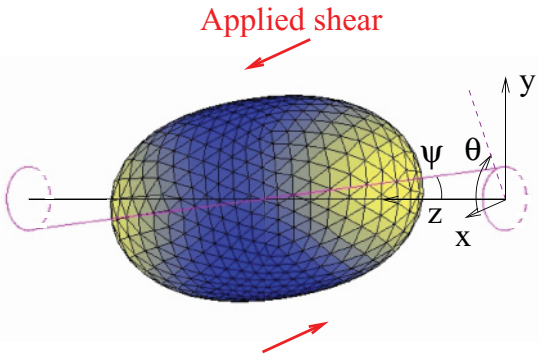

FIG. 7. (Color online) A shape of a vesicle in the K regime showing the the two angles of K. The parameters are $\tau = 0.95$, $C_\kappa = 5$, $\lambda = 20$.

dynamical mode (TB, VB, or K) (only minor variations by few percent are manifested over a range of a decade in shear rate). This finding is not intuitive in as much as deformation (at large enough C_κ) plays an essential role (strong deviation from the KS theory). This result seems not to agree quantitatively with previous numerical analysis [22]. The ratio of their frequency over the KS one undergoes a larger variation (see their Fig. 2) in the explored shear rates, while our results (Fig. 9) show a weak variation.

We have checked that the same quasi-independence on C_κ is also manifested in the new analytical theory [37]. Note that the work of Ref. [22] contains fluctuations that may account for the quantitative difference. Further studies would be needed before a firm conclusion can be reached.

An experimental study on the TB regime has been reported by Mader *et al.* [16]. Their Fig. 5 shows a deviation from the KS theory (their period is larger than the KS period). However, the authors did not report on the actual period, but rather they extracted the period from a fit with the KS theory. Their results are consistent with ours, as explained below.

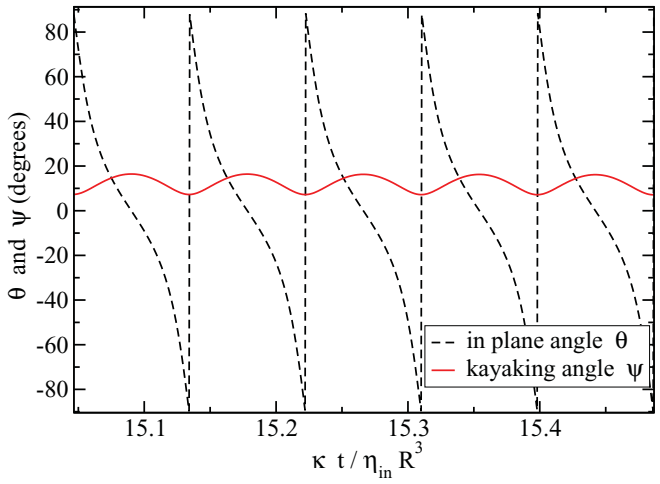

FIG. 8. (Color online) The two angles of K, one in the shear plane measured as a deviation of the major vesicle axis from the flow direction and the other represents the angle of of the cone of the K; the main axis describes a cone about the perpendicular to the plane of the shear flow (see movies [25]). The parameters are $\tau = 0.95$, $C_\kappa = 5$, $\lambda = 20$.

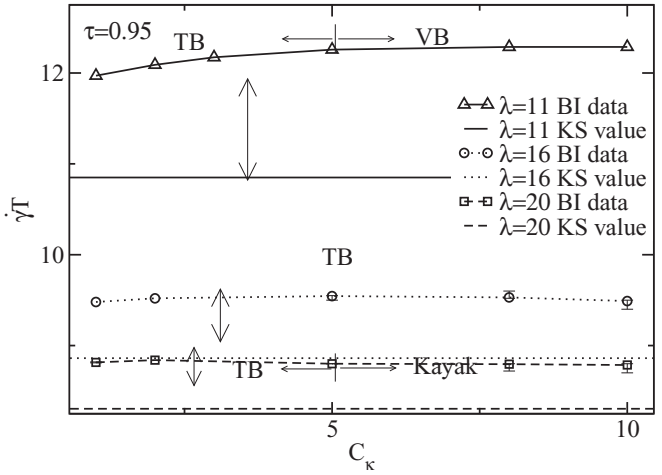

FIG. 9. Rescaled TB period for $\tau = 0.95$ as a function of the deformability C_κ for $\lambda = 11$, 16, and 20.

In order to compare our results with the experimental finding, we must, like experiments, force our data to fit with the KS [17] theory, from which we determine the TB frequency or period. This theory is indeed often used to fit the variations of $\theta(t)$, where t is time, that can be measured experimentally or numerically. In the TB regime, the KS formula [17] is

$$\theta(t) = \arctan\left(\frac{\sqrt{A^2 - B^2}}{A - B}\tan(\sqrt{A^2 - B^2}\, t)\right). \qquad (20)$$

Once the two coefficients A and B are determined, the period is easily obtained as $T = \pi/\sqrt{A^2 - B^2}$. This procedure can be the source of very strong errors when the KS theory becomes inaccurate. We show an example of such a behavior in Fig. 10. This figure shows a fit of $\theta(t)$ with expression (20) for $\lambda = 16$ and $C_\kappa = 11$, where the KS theory is not applicable, as can be easily seen in Fig. 11. It is impressing to see how excellent is the fit in the region where the dynamics is slow ($\theta \in [-\pi/4, \pi/4]$) in Fig. 10. This region is indeed the experimentally accessible one; outside this interval the variation is so fast that usually no point can be measured. Thanks to the very small time step used numerically the full curve $\theta(t)$ is easily obtained (the solid line of Fig. 10). While the true period $\dot\gamma T = 9.5$, the fit with the KS formula gives $\dot\gamma T = 11.3$, which corresponds to an overestimation of the period by 20%. A good fit of the data for $\theta \in [-\pi/4, \pi/4]$ is not a good criterion to test the validity of the KS theory. To show the variation of the fitted period with the deformability, we compare the true period to the result of the fitting procedure for $\lambda = 16$ and C_κ between 1 and 11 in Fig. 12. While the true period remains nearly constant, the period obtained with the KS theory exhibits an apparent rapid growth with C_κ. This increase is an artifact of the fitting procedure. Note that in another (theoretical) paper by Mader *et al.* [38] a toy model was presented. There the authors (their Fig. 5) have (as done in experiments) fitted their data with the KS theory. Their period obtained from the fit shows the same trend as reported here (the crosses in Fig. 12), and more interestingly it varies by about 30% (a variation which is close to what found here) before it

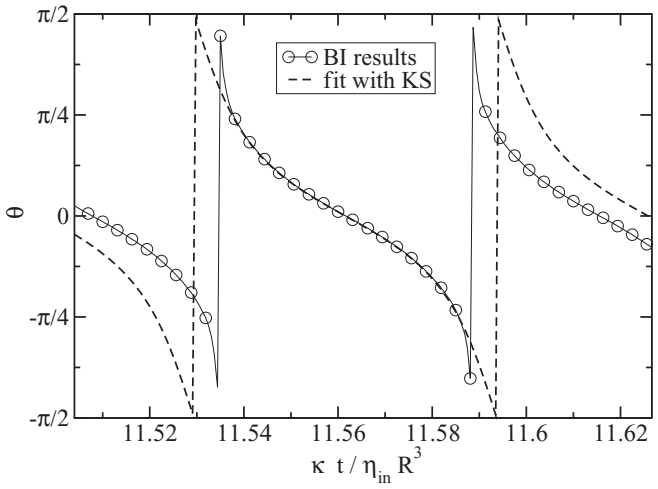

FIG. 10. θ as a function of time (t) for $\lambda = 16$, $C_\kappa = 11$, and $\tau = 0.95$. The dashed line corresponds to a fit with the KS theory. The solid black line with the circles corresponds to the BI simulation. The temporal resolution of the BI simulation corresponds to 400 time steps between two circles. Although the fit seems excellent in the central part of the graph, the period given by this fit is 20% larger than the true one.

saturates at larger C_κ (saturation that occurs in our numerical simulations at about $C_\kappa = 20$ is not shown here).

Finally, it is worth emphasizing that the transient dynamical regime can prove to be very slow, especially at large values of C_κ. It is necessary to ascertain the establishment of a given regime on the scale of the longest time. For large enough λ, the appropriate (slow) time scale is $\tau_\kappa = \eta_{\rm in} R^3/\kappa$; motion is limited by the more viscous internal fluid. For $C_\kappa = 10$, this may typically represent a hundred cycles in the TB regime. Here it suffices to provide an illustration exhibiting the slow relaxation (Fig. 13). The VB amplitude close to the TT-VB line ($\lambda = 9$, $C_\kappa = 8$) is shown. We find an exponential relaxation

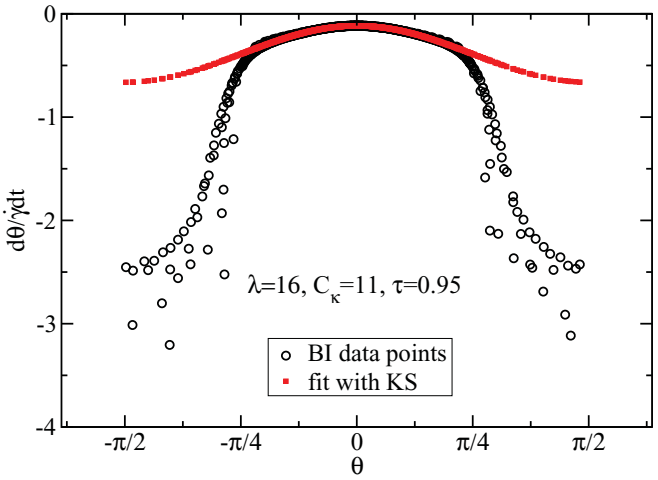

FIG. 11. (Color online) $\dot\theta$ as a function of θ for $\lambda = 16$, $C_\kappa = 11$, and $\tau = 0.95$. The circles are the BI results, while the squares correspond to the fit with the KS theory for $\theta \in [-\pi/4, \pi/4]$. We clearly see that higher harmonics not included in the KS theory are present.

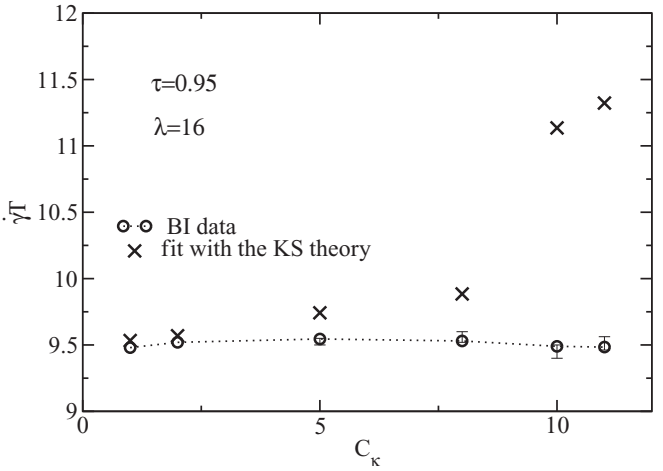

FIG. 12. Rescaled TB period for $\tau = 0.95$ as a function of the deformability C_κ for $\lambda = 16$. The circles are the BI simulation results while the crosses correspond to the fit with the KS theory. The fitted period increases rapidly with C_κ while the true period is almost constant.

of the VB amplitude. The vesicle reaches its steady state only after a characteristic time of about $30\eta_{\rm in}R^3/\kappa$, corresponding to 125 oscillations. This critical slowing down was also discussed analytically in Ref. [21]. Note that it is likely very hard to approach the transition boundary in experiments, due in particular to fluctuations. Membranes' thermal fluctuations will probably affect the location of the boundaries in the phase diagram. Experiments [32,33] report that fluctuations are important for the type of vesicles that were studied, and they show that third-order harmonics is excited. Nevertheless, experiments have attempted a systematic comparison with Lebedev *et al.* [21] analysis which does not include any fluctuation. Inclusion of fluctuations in a future theory should be essential to guide experiments. If one takes parameters away from the bifurcation line, then the relaxation time toward the final regime is shorter (see Fig. 14), of order of few τ_κ's.

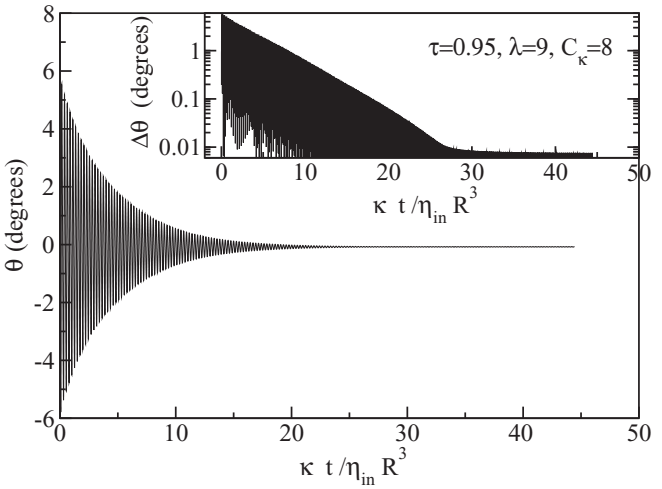

FIG. 13. Long time relaxation of the vesicle close to the TT-VB line. The inset shows a log plot of the vacillation amplitude.

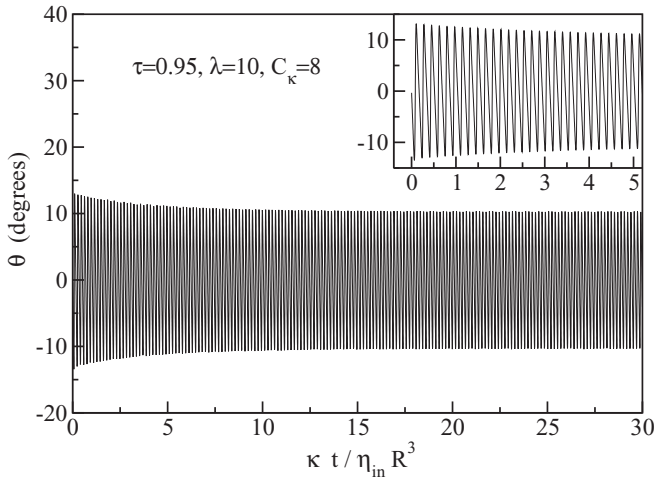

FIG. 14. Relaxation of the vesicle inside the VB region. The inset shows a plot of the vacillation amplitude at small time revealing that an ellipsoid initially oriented along the flow reaches the VB regime quite quickly.

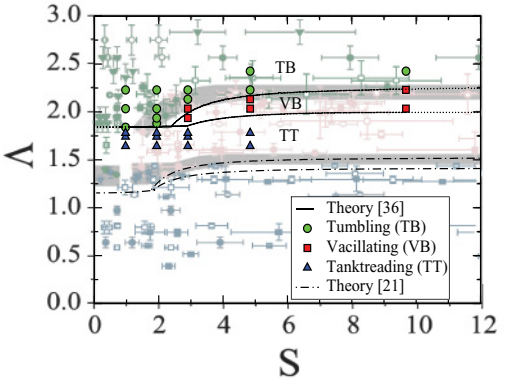

FIG. 15. (Color online) Comparison with the experimental phase diagram by Deschamps *et al.* [32]. The symbols carrying error bars correspond to experimental data of Deschamps *et al.* [32] where the gray bands are guides for the eye (drawn in Ref. [32] in order to delimit the region of the VB mode, called there TR, or trembling). The blue triangles, green circles, and red squares are results from the present numerical simulations. Also shown is the theory by Farutin *et al.* [37] (solid line) and the theory of Lebedev *et al.* [21] (dashed-dotted lines).

Experiments [32] have reported on the time scale of transition from TT to VB (called TR there) and TT to TB. As can be seen from their Fig. 5, it is not easy to state that the amplitude of TR or TB has reached a permanent regime. In addition, no statistics is provided, so that it is difficult to extract a precise time scale. Nevertheless, if we admit that the permanent regime is reached then the time scale is of about few periods, and this is in a reasonable agreement with our data of Fig. 14, where the relaxation time if of about ten periods; note that after the first three periods of our inset of our Fig. 14 the amplitude varies by only few percent, so that it is hard to detect experimentally these small amplitude variations given intrinsic experimental error bars.

V. COMPARISON BETWEEN THE PRESENT PHASE DIAGRAM AND THE EXPERIMENTAL ONE

It is always difficult to compare simulation data with experiments, especially in the context of quasispherical vesicles, as discussed above, but it is tempting to superimpose our phase diagram for $\tau = 0.95$ with the very nice phase diagram obtained experimentally in [32]. This comparison is found in Fig. 15. It is important to mention that the experimental diagram includes vesicles with different reduced volumes, and the phase boundaries are thus necessarily broader than the theoretical ones, obtained for $\tau = 0.95$. The parameters Δ, Λ, and S used in [32] are defined as

$$\Delta = 4\pi(\tau^{-2/3} - 1), \quad \Lambda = \frac{4\sqrt{\Delta}}{\sqrt{30\pi}}\left(1 + \frac{23}{32}\lambda\right), \quad S = \frac{7\pi}{3\sqrt{3}\Delta}C_\kappa. \tag{21}$$

These variables originate from the early theoretical approaches [21] that predicted a phase diagram with no dependence in Δ (τ in our variables). To make clear that the phase diagram indeed depends on τ, meaning that in total three dimensionless parameters are relevant, in contrast to the single available experimental report [32], we present the phase diagram for $\tau = 0.95$ and $\tau = 0.8$ (Figs. 16 and 17) in the rescaled variables Λ and S. We can easily see that the two phase diagrams differ, and more specifically the VB phase is shifted upward when τ decreases. The same behavior is recovered by the analytical calculation [37]. Note also that the VB band in the numerical data (Fig. 17) lies above the VB experimental band, meaning that for this value of excess area (about 2) our band is shifted upward by about a factor 1.7 on the average. Furthermore, according to the experimental data it is likely that thermal fluctuations play a significant role. Inclusion of thermal fluctuations should constitute an interesting step

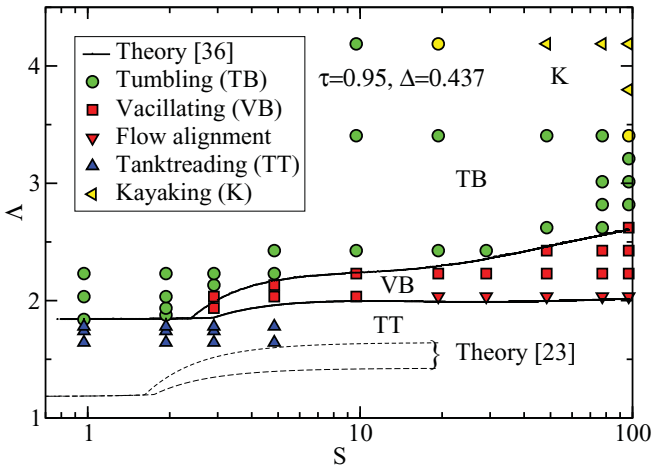

FIG. 16. (Color online) Phase diagram for $\tau = 0.95$ in the variables Λ and S. Numerical simulations are represented with symbols. Also shown are the theory of Danker *et al.* [23] (dashed line) and of Farutin *et al.* [37] (solid line).

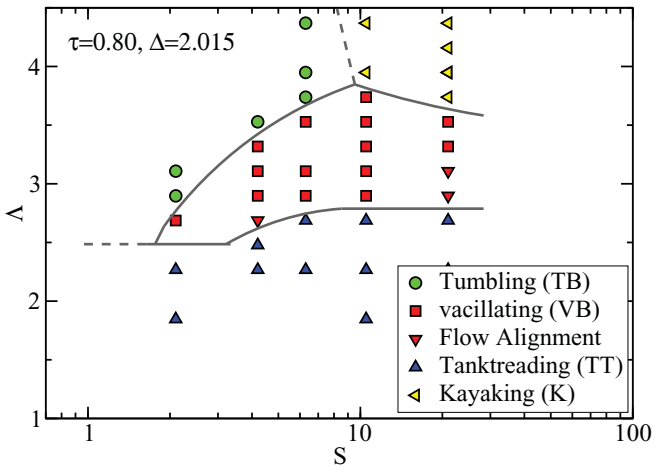

FIG. 17. (Color online) Phase diagram for $\tau = 0.80$ in the variables Λ and S. The scale is identical to the scale of Fig. 16. The solid and dashed lines are guide for the eyes.

toward a more complete comparison between theory and experiments.

VI. COMPARISON BETWEEN EXPERIMENTS AND THE NUMERICAL CALCULATION IN THE TANK-TREADING REGIME

The TT regime of vesicles has been investigated experimentally in Ref. [24] for different excess area (or reduced volume). We would like to compare their results to ours. We represent the results in terms of the variable Λ defined above. This choice is made in order to compare with the results of Ref. [21], where it was suggested that in the TT regime the TT angle would practically depend on a single parameter only, namely Λ. Indeed, the second parameter S plays almost no role, since its value is of about 400 (recall that $C_\kappa = 100$) and,

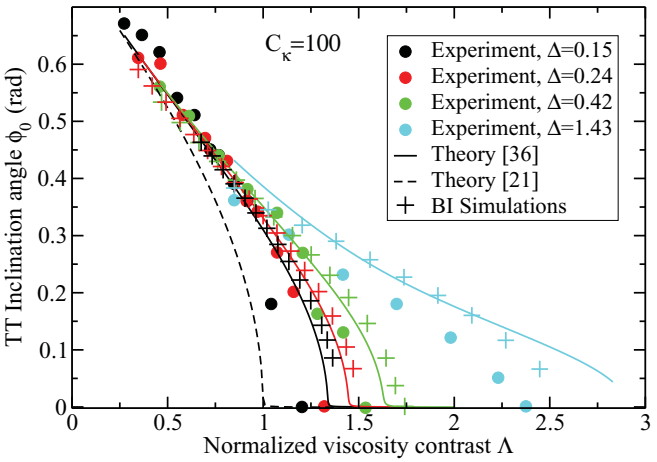

FIG. 18. (Color online) The TT angle as a function of Λ for different excess area. We compare experimental data of Kantsler and Steinberg [24] (their Fig. 2 where data are converted in terms of the variable Λ) versus simulations and theories of Lebedev *et al.* [21] and Farutin *et al.* [37].

from the equations of Ref. [21] in the TT regime, one can easily see that the correction to the TT angle is of about $1/S$. The various results (theory, present simulations, and experiments) are reported in Fig. 18 for the different excess area from a sphere explored experimentally [24]. The results show a rather satisfactory agreement between the present work and experiments. Some deviations are found, however, at small angles. It is likely that in the small angle regimes thermal fluctuations (together with inherent difficulty in estimating the angle) may explain these deviations. A firm conclusion on the origin of deviations at small angles is at present not achieved yet. The experimental data reported in Fig. 18 are extracted from Fig. 2 of [24]. In a later paper by the same group [32] some discussion about error bars is presented. However, the authors did not provide any new figure replacing Fig. 2 of their earlier publication [24].

Another important remark is that both experiments and the present simulations show that the TT angle depends, besides Λ, on the excess area from a sphere. From the experimental data (as well as from the simulations), it is seen that the position of the zero angle (which is very close to the bifurcation point toward the VB mode at large enough $C\kappa$, the experimentally explored range; we have set $C_\kappa = 100$) depends significantly on the excess area.

VII. CONCLUSION

We have reported on a quantitative numerical analysis in three dimensions that led us to identify new features of vesicle dynamics, which were not revealed in prior analytical, numerical, or experimental studies. We have discussed the four types of motions, namely, TT, TB, VB, and K. We have found that the dynamics (as well as the phase diagram) is sensitive to three dimensionless parameters, and not only two, as reported in [21,32,33]. Our finding agrees with the analytical theory [37] in the small excess area limit (the range of applicability of the theory). The TB period rescaled by the shear rate is found to be quite insensitive to the shear rate, in good agreement with the KS theory. In the vicinity of the K mode large deviations of the KS equation $\dot{\theta}/\dot{\gamma} = A + B\cos(2\theta)$ are found.

Our vesicle model has considered the standard ingredients: Stokes flow with viscosity contrast, bending rigidity, and membrane incompressibility. Other effects have not been included here and should constitute interesting tasks for future investigations: (i) What is the influence of thermal fluctuations? (ii) What is the role of the spontaneous curvature? (iii) what are the effect of the membrane internal dissipation (i.e., by considering the possibility that the two membrane monolayers slide with respect to each other) and the membrane viscosity?

Finally, regarding RBC dynamics and blood rheology, an obvious limitation of our work is the absence of shear elasticity associated with the cytoskeleton. An analysis that includes this factor constitutes the next natural step.

ACKNOWLEDGMENTS

C.M. and A.F. acknowledge financial support from CNES and ANR (MOSICOB project).

[1] G. Danker and C. Misbah, Phys. Rev. Lett. **98**, 088104 (2007).
[2] M. Kraus, W. Wintz, U. Seifert, and R. Lipowsky, Phys. Rev. Lett. **77**, 3685 (1996).
[3] I. Cantat and C. Misbah, Phys. Rev. Lett. **83**, 235 (1999).
[4] T. Biben and C. Misbah, Phys. Rev. E **67**, 031908 (2003).
[5] C. Pozrikidis, Ann. Biomed. Eng. **31**, 1 (2003).
[6] A. Diaz and D. Barthès-Biesel, Comput. Model. Eng. Sci. **3**, 321 (2002); E. Lac, A. Morel, and D. Barthès-Biesel, J. Fluid Mech. **149**, 573 (2007).
[7] H. Noguchi and G. Gompper, Phys. Rev. Lett. **93**, 258102 (2004).
[8] Y. Liu and W. K. Liu, J. Comput. Phys. **220**, 139 (2006).
[9] M. M. Dupin, I. Halliday, C. M. Care, L. Alboul, and L. L. Munn, Phys. Rev. E **75**, 066707 (2007).
[10] S. K. Veerapaneni, D. Gueyffier, D. Zorin, and G. Biros, J. Comput. Phys. **227**, 1739 (2008).
[11] P. Bagchi and R. M. Kalluri, Phys. Rev. E **80**, 016307 (2009).
[12] D. A. Fedosov *et al.*, Biophys. J. **98**, 2215 (2010).
[13] H. L. Goldsmith and J. Marlow, Proc. R. Soc. London B **182**, 351 (1972); T. Fischer, M. Stohr-Lissen, and H. Schmid-Schonbein, Science **202**, 894 (1978); M. Bitbol, Biophys. J. **49**, 1055 (1986); M. Abkarian, M. Faivre, and A. Viallat, Phys. Rev. Lett. **98**, 188302 (2007).
[14] K. H. de Haas, C. Blom, D. van den Ende, M. H. G. Duits, and J. Mellema, Phys. Rev. E **56**, 7132 (1997).
[15] V. Kantsler and V. Steinberg, Phys. Rev. Lett. **95**, 258101 (2005).
[16] M.-A. Mader, V. Vitkova, M. Abkarian, A. Viallat, and T. Podgorski, Eur. Phys. J. E **19**, 389 (2006).
[17] S. R. Keller and R. Skalak, J. Fluid Mech. **120**, 27 (1982).
[18] U. Seifert, Eur. Phys. J. B **8**, 405 (1999).
[19] C. Misbah, Phys. Rev. Lett. **96**, 028104 (2006).
[20] P. M. Vlahovska and R. S. Gracia, Phys. Rev. E **75**, 016313 (2007).
[21] V. V. Lebedev, K. S. Turitsyn, and S. S. Vergeles, Phys. Rev. Lett. **99**, 218101 (2007); New J. Phys. **10**, 043044 (2008).
[22] H. Noguchi and G. Gompper, Phys. Rev. Lett. **98**, 128103 (2007).
[23] G. Danker, T. Biben, T. Podgorski, C. Verdier, and C. Misbah, Phys. Rev. E **76**, 041905 (2007).
[24] V. Kantsler and V. Steinberg, Phys. Rev. Lett. **96**, 036001 (2006).
[25] See supplemental material at [http://link.aps.org/supplemental/10.1103/PhysRevE.83.031921] for dynamics of a vesicle under shear flow in the TT, TB, VB, and K regimes.
[26] G. B. Jeffery, Proc. R. Soc. London A **102**, 161 (1922).
[27] P. Pasin *et al.*, eds., in *Computer Simulations of Liquid Crystals and Polymers*, NATO Science Series II, Vol. 177 (Springer, New York, 2005).
[28] C. Pozrikidis, *Boundary Integral and Singularity Methods for Linearized Viscous Flow* (Cambridge University Press, Cambridge, 1992).
[29] O. Y. Zhong-can and W. Helfrich, Phys. Rev. A **39**, 5280 (1989).
[30] G. Taubin, in *Proceedings of the Fifth International Conference on Computer Vision* (ICCV' 95), pp. 852–857.
[31] W. Helfrich, Z. Naturforsch. C **28**, 693 (1973).
[32] J. Deschamps, V. Kantsler, and V. Steinberg, Phys. Rev. Lett. **102**, 118105 (2009).
[33] J. Deschamps, V. Kantsler, E. Segre, and V. Steinberg, Proc. Natl. Acad. Sci. USA **106**, 11444 (2009).
[34] J. M. Skotheim and T. W. Secomb, Phys. Rev. Lett. **98**, 078301 (2007).
[35] U. Seifert, Adv. Phys. **46**, 13 (1997).
[36] H. Noguchi and G. Gompper, Phys. Rev. E **72**, 011901 (2005).
[37] A. Farutin, T. Biben, and C. Misbah, Phys. Rev. E **81**, 061904 (2010).
[38] M.-A. Mader, H. Ez-Zahraouy, C. Misbah, and T. Podgorski, Eur. Phys. J. E **22**, 275 (2007).